X1822-371: When the neutron star lies hidden

Antonino D'Aì
R. Iaria, L. Burderi, T. Di Salvo, N.Robba, A. Papitto, A.Riggio

Dipartimento di Fisica
Universitá di Palermo

Physics of Neutron Stars
St. Petersburg
July 14 2011

dsfa

Basic characteristics

- X1822-371 is a compact binary system with a period of 5.57hr, seen almost edge-on (inclination $82.5^\circ \pm 1.5^\circ$) at a distance of 2.5 kpc.
- The X-ray light curve is periodically modulated, presenting both dips and eclipse.
- It is considered the prototype of the Accretion Disk Coronae (ADC) Sources (White & Holt, 1982).
- The compact object is a NS with a spin period of 0.56 s.
- The broadband X-ray spectrum is relatively soft (cut-off at 4-5 keV) with an apparent luminosity of $\sim 10^{36}$ erg s^{-1}

X 1822-371

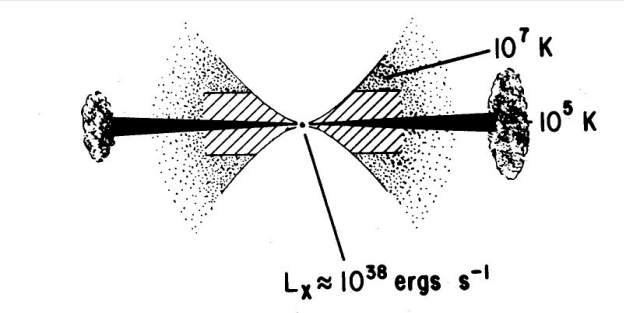

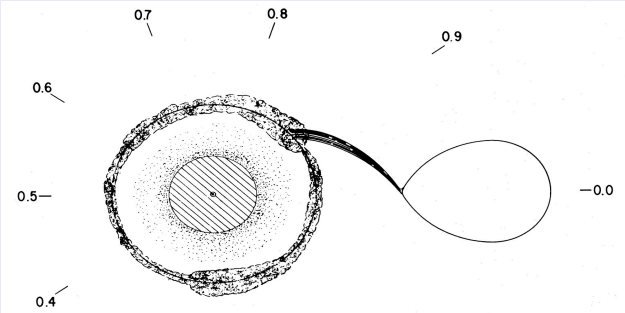

The dipping class: evidence for hot coronae

Optically thick coronae

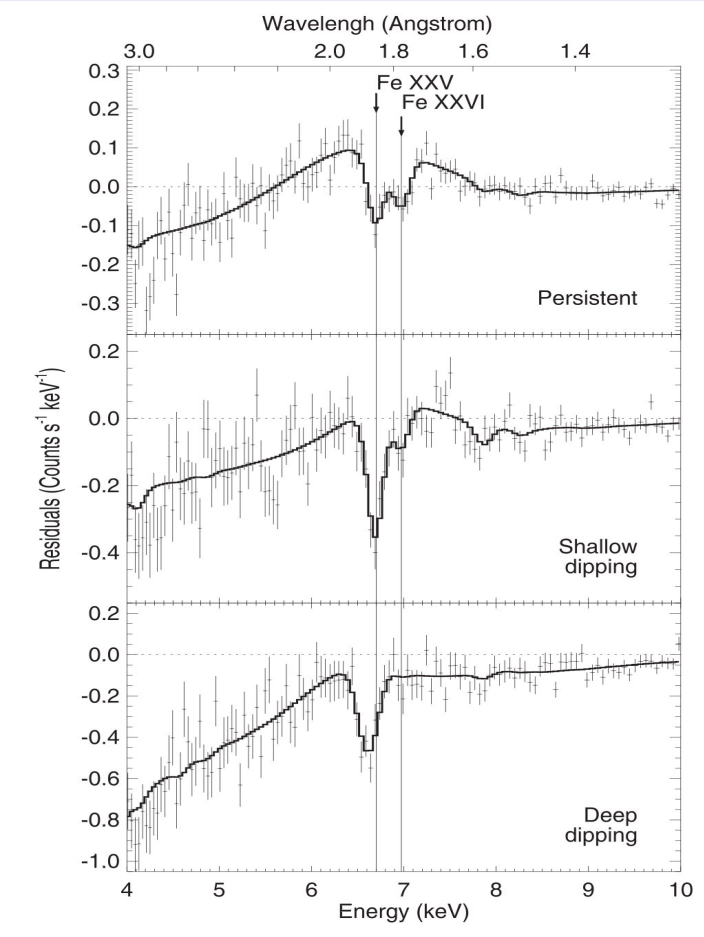

4U 1323-62; Boirin et al. 2005

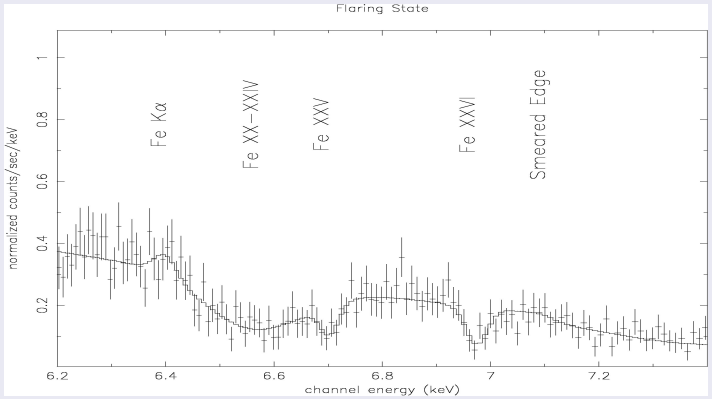

Cir X-1; D'Aì et al. 2007

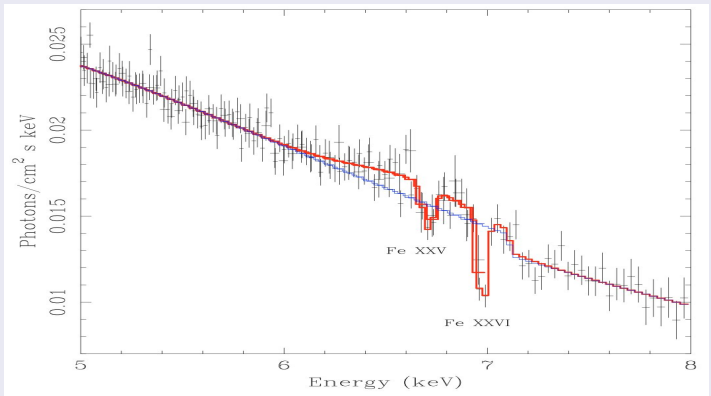

X 1624-49; Iaria et al. 2007

The orbital period evolution

Eclipse timing delays: a long-lasting effort

- *Hellier et al. (1990)The ephemeris of X1822-371*
- Parmar et al. (2000)*Beppo-Sax observation of X1822-371*
- Burderi et al. (2010) *A stable orbital period derivative over 30 years*
- Iaria et al. (2011) *X-ray and Optical-UV ephemeris*

Time delays

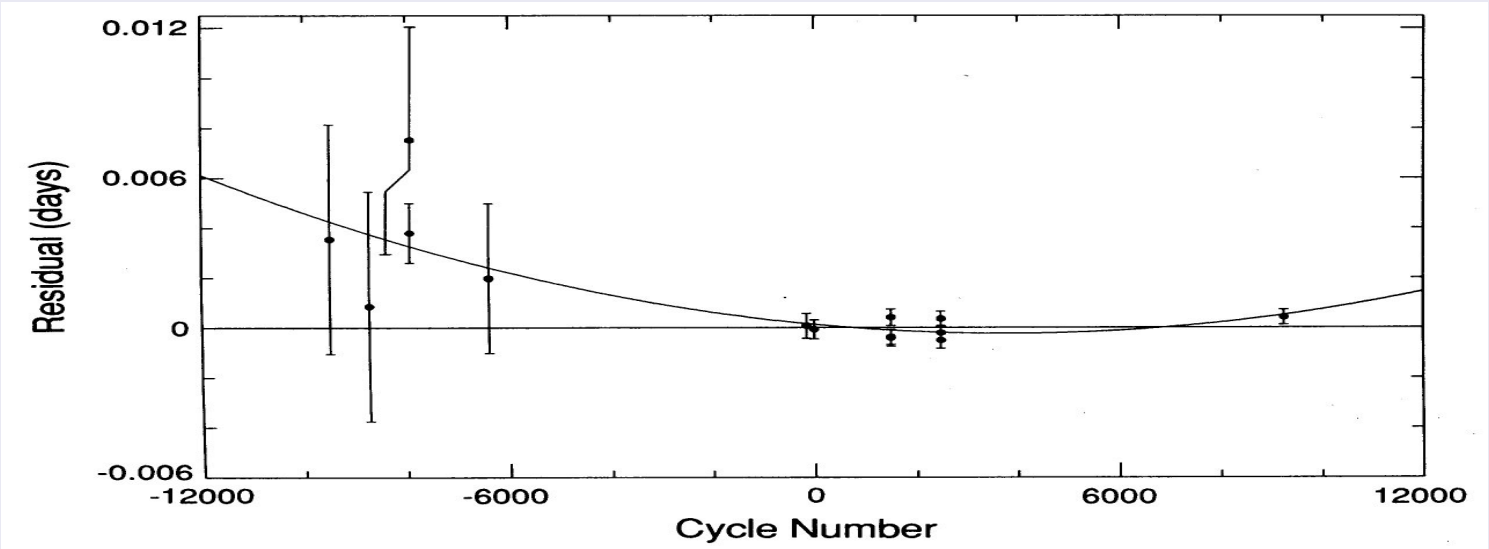

The orbital period evolution

Eclipse timing delays: a long-lasting effort

- Hellier et al. (1990) *The ephemeris of X1822-371*
- *Parmar et al. (2000)Beppo-Sax observation of X1822-371*
- Burderi et al. (2010) *A stable orbital period derivative over 30 years*
- Iaria et al. (2011) *X-ray and Optical-UV ephemeris*

Time delays

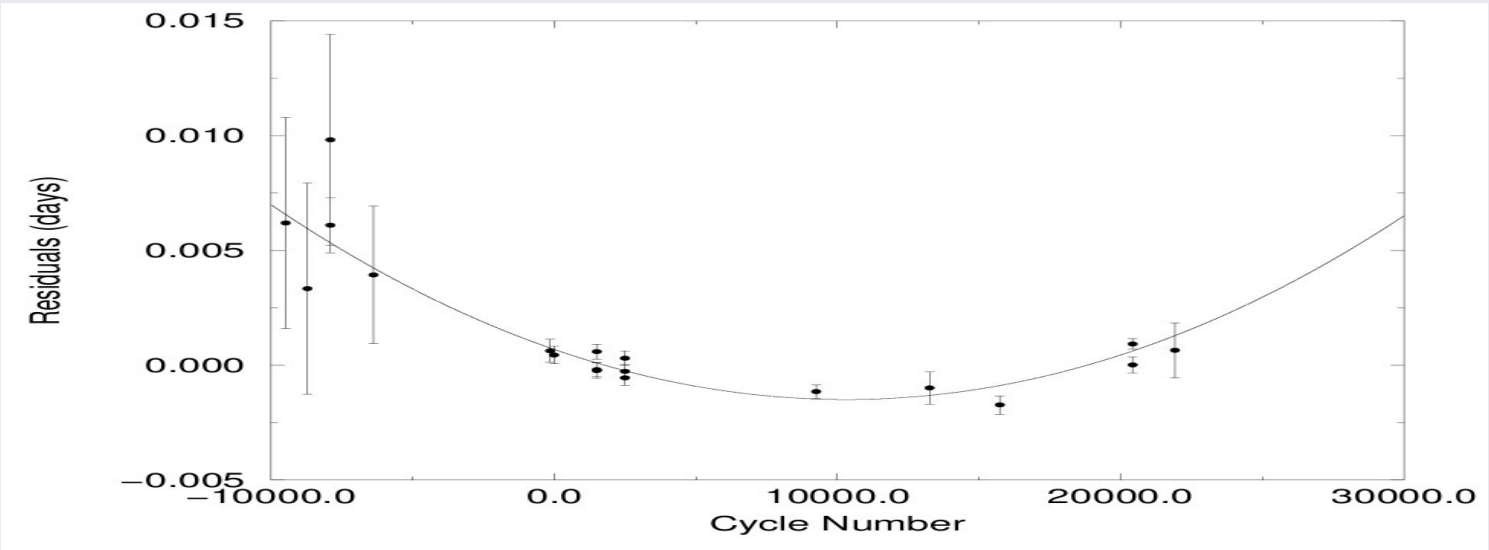

The orbital period evolution

Eclipse timing delays: a long-lasting effort

- Hellier et al. (1990) *The ephemeris of X1822-371*
- Parmar et al. (2000) *Beppo-Sax observation of X1822-371*
- *Burderi et al. (2010) A stable orbital period derivative over 30 years*
- Iaria et al. (2011) *X-ray and Optical-UV ephemeris*

Time delays

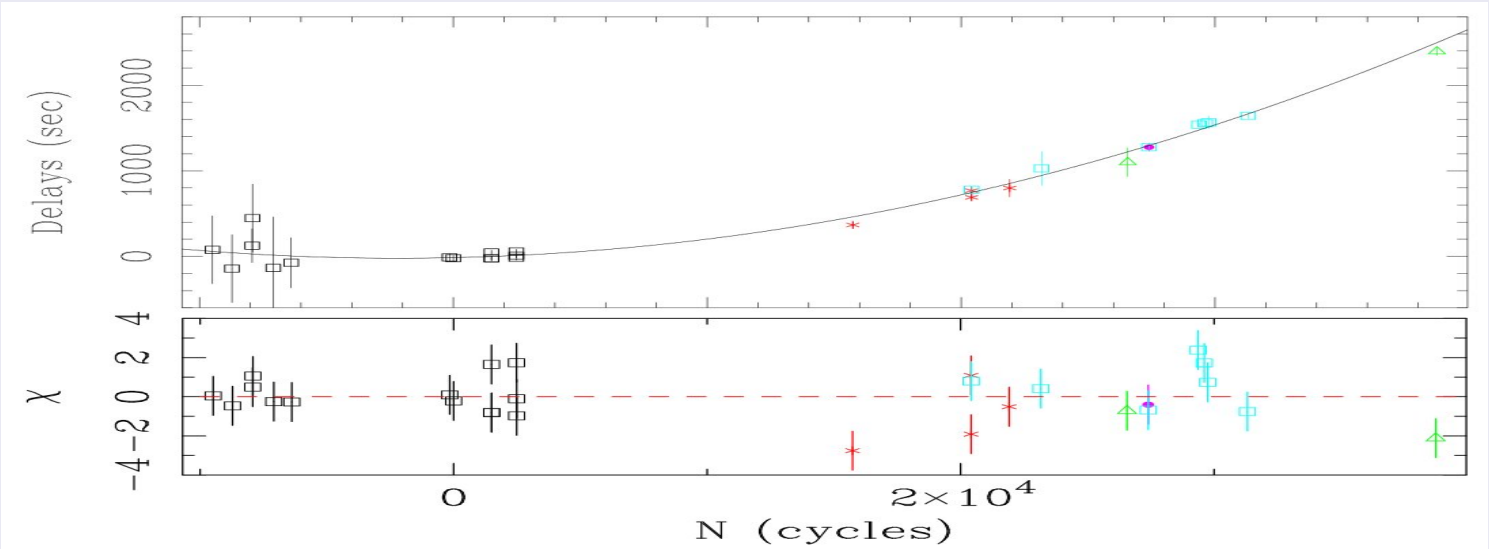

The orbital period evolution

Eclipse timing delays: a long-lasting effort

- Hellier et al. (1990) *The ephemeris of X1822-371*
- Parmar et al. (2000) *Beppo-Sax observation of X1822-371*
- Burderi et al. (2010) *A stable orbital period derivative over 30 years*
- *Iaria et al. (2011) X-ray and Optical-UV ephemeris*

Time delays

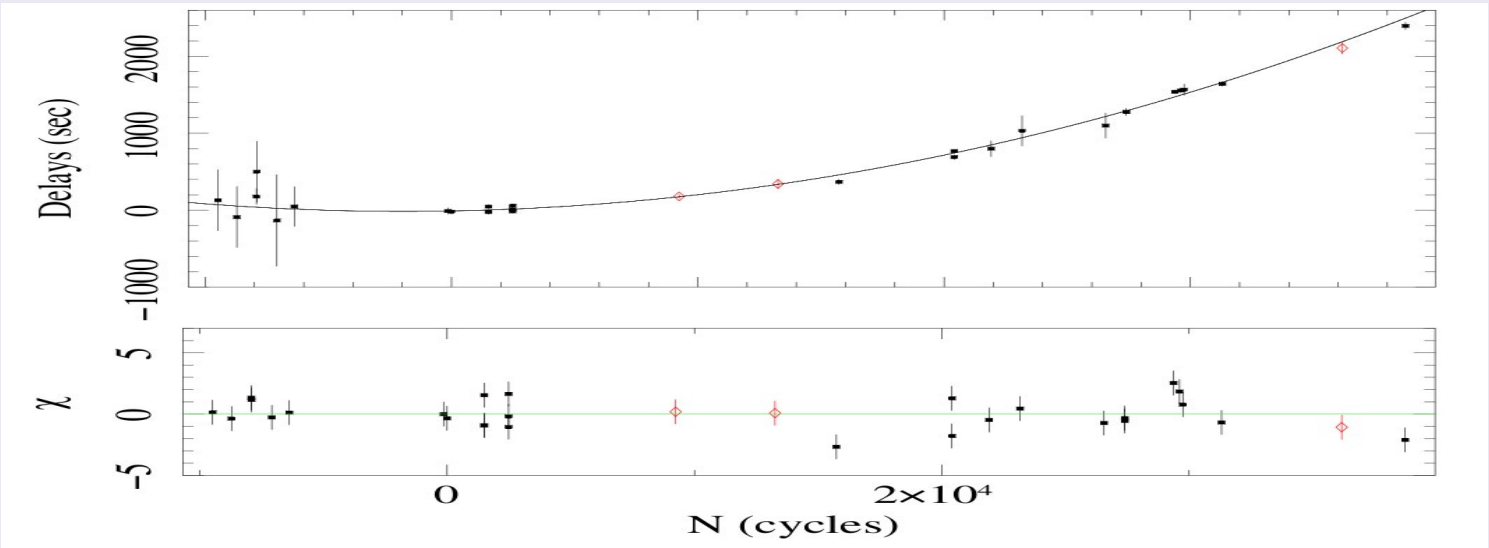

X-ray and optical ephemeris: time-lag and periodicities

We performed a comprehensive reanalysis of all the eclipse timing delays across all the available wavebands (X-ray, optical-UV).
Extension of the work of Burderi et al. (2010) and Bayless et al. (2010).

Time delays

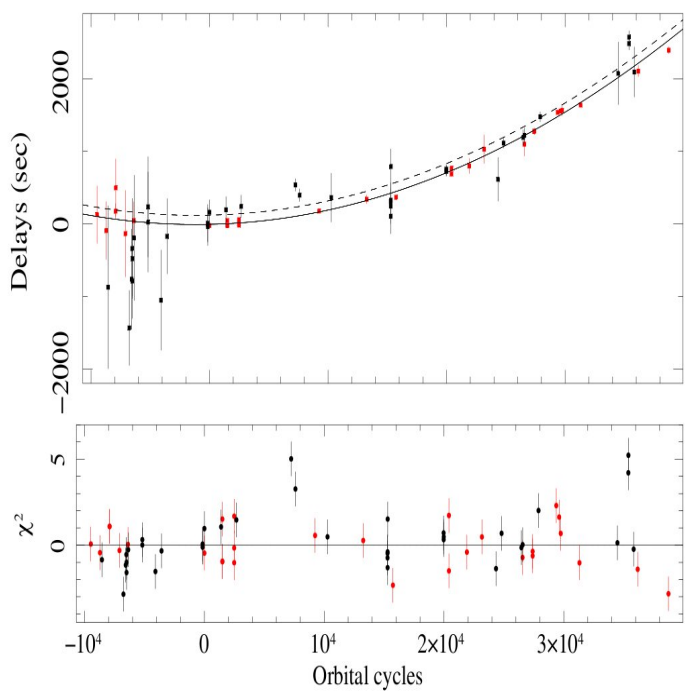

Constrained X-ray and optical-UV ephemeris:

- T_0 = 45614.80957(19) MJD
- P_{orb} = 20054.2027(28) s
- $\dot{P}_{orb}$ = 1.591(86) $\times$ 10^{-10} s/s
- ΔT_{lag} = 127 $\pm$ 52 s (2.4 σ detection)
- χ^2/dof = 124/62

dsfa

Optically modulated time-lags?

We investigated on the possibility of a periodicity in the time-lags amplitude of the UV-optical eclipse time passages with respect to the X-ray eclipse time passages, obtaining two equivalent best-fit solutions.

6593±450 days

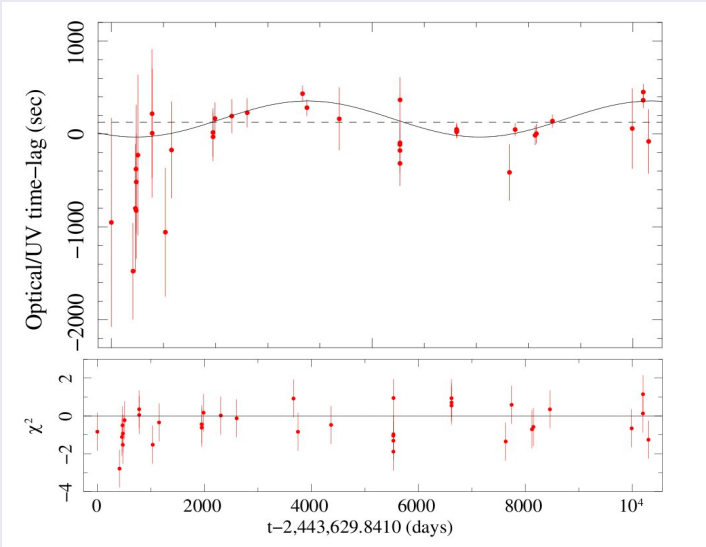

Time-lag: 161± 24 s
Amplitude: 194 ± 25 s

283.1±0.6 days

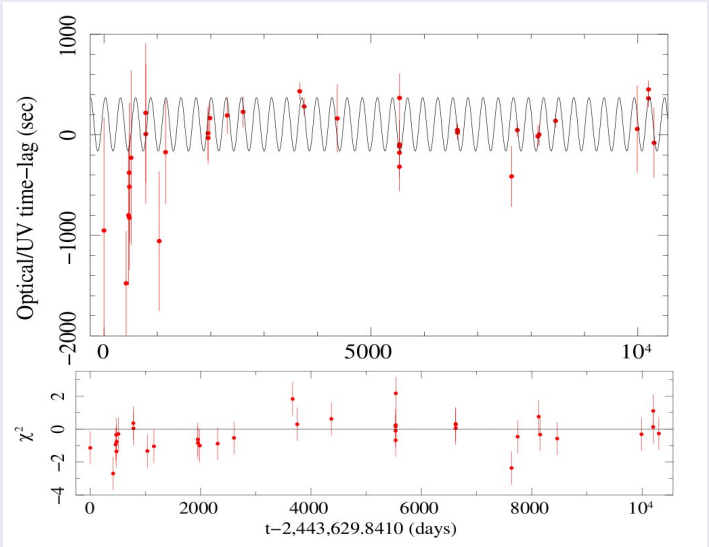

Time-lag: 105± 24 s
Amplitude: 267 ± 43 s

But superhump and beat frequency do not work...

dsfa

The large period derivative

Angular momentum losses

30 years of timing have set on solid ground the determination of the orbital period derivative ($\dot{P}_{orb} = 1.591(86) \times 10^{-10}$ s/s). This value is extremely large. Where are the reasons for it?

- Under *conservative mass-transfer* conditions, the only effects that can play a role in raising the orbital period derivative are: **magnetic braking effects** and **gravitational wave emission**

but, even under the most favourable conditions, these two effects are not sufficient to keep a conservative mass-transfer scenario (see Burderi et al. 2010).

So, how to resolve this dilemma? Non-conservative super-Eddington regime

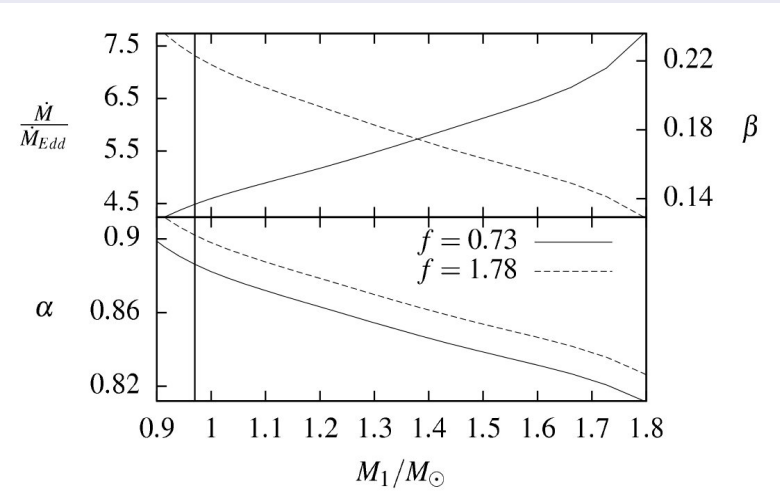

where β = mass fraction accreted by the NS; α = specific angular momentum of the mass expelled in units of the specific angular momentum of the secondary; f = 0.73 MB prescription according to Skumanich (1972) and f = 1.78 according to Smith (1979).

dsfa

A detailed analysis on the physical properties of the ADC

Our theoretical scenario and the spectral analysis

We present here a preliminary analysis of the 0.5-10 keV X-ray spectrum using:

- Two Chandra HETGS observations of 66 ks and 84 ks (Iaria, D'Aì et al. 2011, A&A submitted)
- A XMM-Newton observation of 53.8 ks (Iaria, D'Aì et al. 2011, A&A submitted)
- A Suzaku observation of 88 ks (D'Aì et al. 2011, in preparation)

A toy-model to esteem basic physical parameters

Since the observed luminosity is only $\sim 10^{36}$ erg s^{-1}, instead of the expected Eddington luminosity ($\sim 2 \times 10^{38}$ erg s^{-1}), we propose that the observed emission is only the scattered emission from the corona, while the neutron star emission (the emission within the magnetosphere) is totally shielded.
If the ADC is assumed spherical, centered on the NS where the main physical process under consideration is Thomson scattering, we have:

$$L_{sc} = L_0 - L_{uns} = L_0(1 - e^{-\tau}) \simeq L_o\tau \tag{1}$$

if we assume $\tau << 1$. The observed flux (Φ_{obs}), according to our hypothesis, entirely corresponds to the scattered flux (Φ_{sc}) of the corona, this leads to:

$$\Phi_{sc} = \Phi_{obs} = \frac{L_{sc}}{4\pi D^2} = \frac{L_0\tau}{4\pi D^2} \tag{2}$$

$$\Phi_{obs} = \frac{1.1 \times 10^{36}\ erg\ s^{-1}}{4\pi(2.5kpc)^2} = \frac{2 \times 10^{38}\ erg\ s^{-1}\tau}{4\pi D^2} \tag{3}$$

$$\tau = 5.5 \times 10^{-3} \tag{4}$$

dsfa

The size of the corona

V_{obs} can be approximated by a cylinder of base πR_{L2}^2 and height 2 R_c. The visible volume V_{vis}

$$V_{vis} = \frac{4}{3}\pi R_c^3 - 2\pi R_{L2}^2 R_c \tag{5}$$

The emissivity of the ADC, since it only depends on the primary flux at a distance r from the source, can be written as:

$$\epsilon = \frac{L_0 n_e \sigma_T}{4\pi r^2} \tag{6}$$

$$\int_{V_{tot}} \epsilon(r)dV = \int_{V_{vis}} \epsilon(r)dV + \int_{V_{obs}} \epsilon(r)dV \tag{7}$$

Calculations lead to:

$$\frac{\Phi_{ecl}}{\Phi_{pers}} = \frac{\int_{V_{vis}} \epsilon(r)dV}{\int_{V_{tot}} \epsilon(r)dV} = \left(1 - \frac{R_{L2}}{R_c}\right) \times \frac{1 - \frac{3}{2}\left(\frac{R_{L2}}{R_c}\right)^2}{1 - \left(\frac{R_{L2}}{R_c}\right)^3} \tag{8}$$

A system's sketch

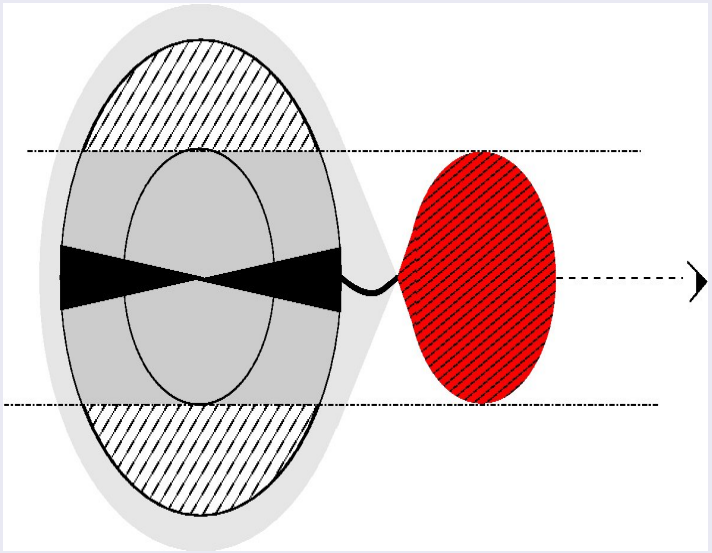

$$R_c \sim 8.8 \times 10^{10} cm. \tag{9}$$

$$n_e = 9.4 \times 10^{10} cm^{-3} \tag{10}$$

dsfa

Maximum time delay in the corona

$$\Delta t \leq 2R_c/c = 6.3s \tag{11}$$

We can define a *coherence radius* (R_{coh}), as the radius at which two scattered photons within the corresponding sphere, would still preserve coherence.

$$\frac{L_{coh}}{L_{uncoh}} \approx \frac{R_{coh}}{R_c} \tag{12}$$

Inside the coherence sphere the maximum time delay between two scattered photons is $\Delta T_{coh} \leq 2R_{coh}/c$. We can set a condition on the size of the coherence radius by imposing a maximum time delay (Δt_{max}, e.g. $< 20\%$ of the pulse period).

$$\Delta t_{max} \sim 0.4P_{spin} \rightarrow \frac{2R_{coh}}{c} \sim 0.4P_{spin} \rightarrow R_{coh} = 3.54 \times 10^9 \ cm \tag{13}$$

where the factor 2 comes from the fact that the mean time delay $\overline{\Delta t} = \frac{1}{2}\Delta t_{max}$.

The pulsed fraction II

Derivation of the pulsed fraction

$$Pf_{obs} = \frac{R_{coh}}{R_c} \times Pf_{int} \quad (14)$$

where Pf_{int} is the intrinsic pulsed fraction.
Since Pf_{int} is < 1, we have:

$$Pf_{obs} < \frac{R_{coh}}{R_c} \sim 4\% \quad (15)$$

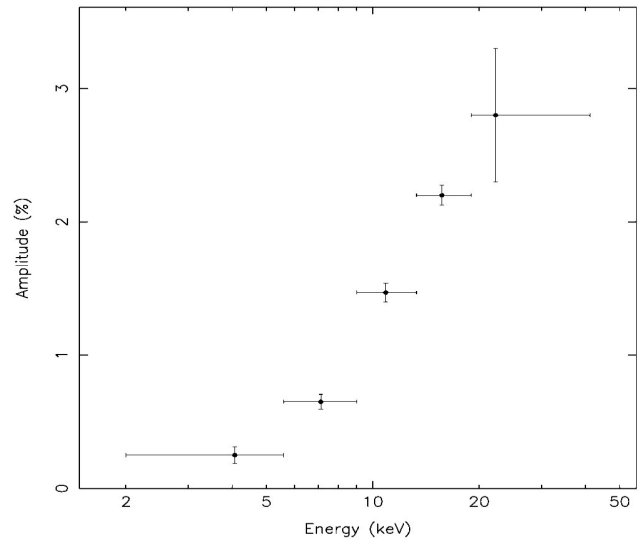

Reference

Jonker & Van der Klis, ApJ, 2001

dsfa

The phase-averaged spectrum: the continuum emission

The continuum model

We fitted the continuum emission adopting the model proposed by Iaria (2001) for the broad band BeppoSAX spectrum of X1822-371: i.e. a Comptonised component (`Compst` in XSPEC) partially absorbed by neutral matter (`pcfabs` in XSPEC) and absorbed by interstellar matter (`wabs` in XSPEC).

Results

Both *Chandra* and *XMM-Newton* spectra are satisfactorly well fitted by this model and best-fitting model parameters are consistent between the two spectra. The Comptonized emission is optically thick, most probably originated within the magnetosphere of the accreting pulsar. This emission is partially occulted by an extended envelope of cold matter. We observe a modulation of the flux of the `Compst` component, *while the spectral shape does not depend on the orbital phase.*

Best-fitting model parameters

Averaged Spectrum. Best-fitting values of the Continuum emission.

Parameters	HETGS	XMM
N_H (10^{22} cm^{-2})	0.113 ± 0.010	$0.1023^{+0.0011}_{-0.0029}$
$N_{H_{pc}}$ (10^{22} cm^{-2})	3.35 ± 0.13	3.34 ± 0.08
f	0.625 ± 0.015	0.578 ± 0.010
kT_e (keV)	3.1 ± 0.2	2.97 ± 0.04
τ	19.1 ± 0.9	21.1 ± 0.4
N_{Compst}	0.067 ± 0.004	0.0365 ± 0.0010
$\chi^2_{red}(d.o.f.)$	0.68(3478)	1.18(2302)

NOTE — Best-fitting values for the parameters of the continuum component. Uncertainties are at the 90% confidence level (hereafter c. l.) for a single parameter. The parameters are defined as in XSPEC. The continuum emission is fitted with a Comptonised component (`Compst` in XSPEC) partially absorbed by neutral matter. The equivalent hydrogen column of the local neutral matter is indicated with $N_{H_{pc}}$, the covered fraction of the emitting surface is indicated with f.

dsfa

Phase-dependent variations of the spectral parameters

Compst parameters

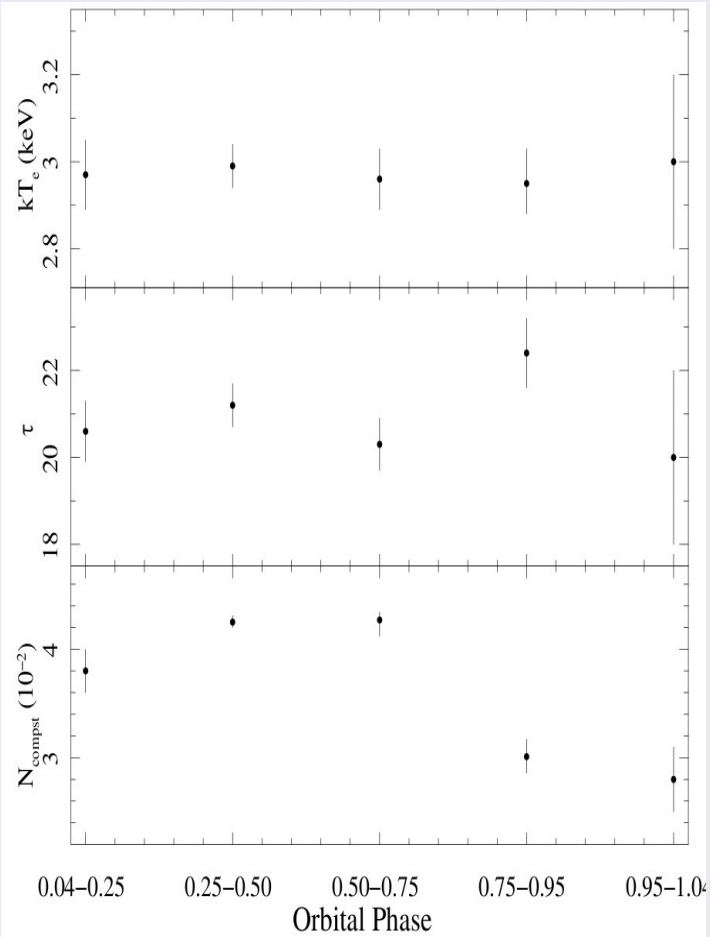

Partial Covering parameters

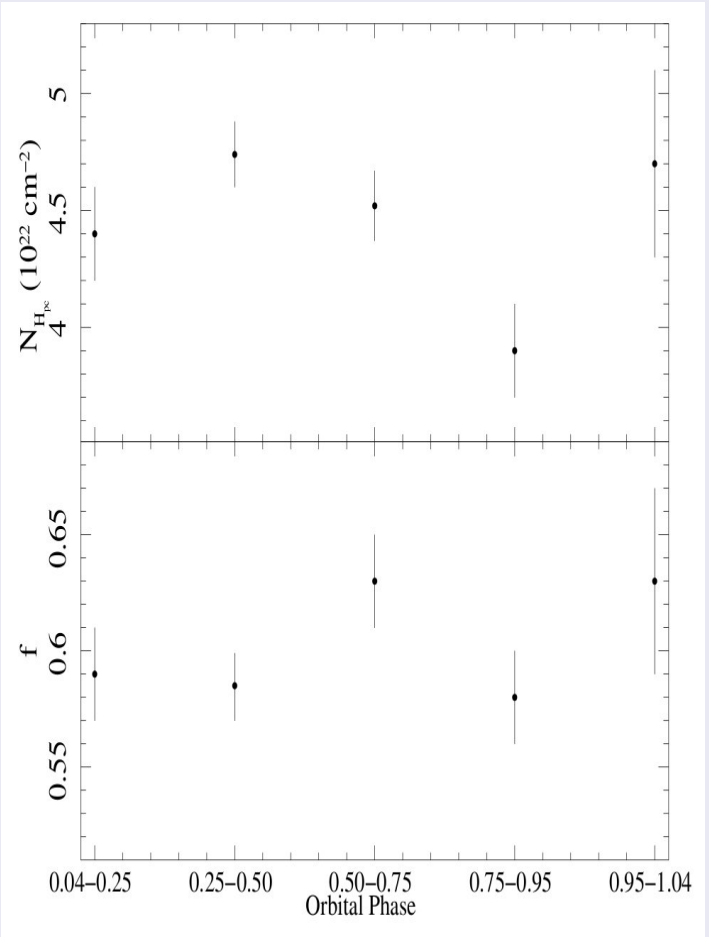

Continuity equation:

$$(1-\beta)\dot{M}_2 = 4\pi r^2 \rho(r) v(r) \zeta \tag{16}$$

Matter ejected at the escape speed (lower limit):

$$v_{esc}(r) = 2\left(\frac{G(M_1+M_2)}{r}\right)^{1/2} \tag{17}$$

$$\rho(r) = 4.7\times 10^3 (1-\beta)(\zeta\eta)^{-1}\dot{M}_2 (M_1+M_2)^{-1/2} r^{-3/2}\ g\ cm^{-3} \tag{18}$$

$$n(r) = 4.5\times 10^{27} (1-\beta)(\zeta\eta)^{-1}\dot{M}_2 (M_1+M_2)^{-1/2} r^{-3/2}\ cm^{-3} \tag{19}$$

$$n(a) \sim 3.1\times 10^{11} (\zeta\eta)^{-1}\ cm^{-3} \tag{20}$$

$$N = 4\times 10^{22} (\zeta\eta)^{-1} cm^{-2} \tag{21}$$

Line spectroscopy

The X-ray spectrum of X1822-371 shows several emission lines. We identify several transitions from H-like and He-like ions. We show here spectroscopic results from the study of He-like triplets of O VII, Ne IX and Mg XI.

Table 3. Best-fitting values of the O VII, Ne IX, and Mg XI triplets.

		E (keV)	σ (eV)	I (10^{-4} ph cm^{-2} s^{-1})
		O VII		
	f	0.5610 (fixed)	1.0 ± 0.2	$0.2^{+3.2}_{-0.2}$
MEG	i	0.5684 ± 0.0002	1.0 ± 0.2	27 ± 5
	r	0.5734 ± 0.0014	1.0 ± 0.2	5 ± 3
	f	0.5610 (fixed)	1 (fixed)	< 0.2
RGS1	i	0.5687 (fixed)	1 (fixed)	15.4 ± 1.0
	r	0.5739 (fixed)	1 (fixed)	1.5 ± 0.7
		Ne IX		
	f	0.9051 (fixed)	1.3 ± 0.2	$0.2^{+0.3}_{-0.2}$
MEG	i	0.9145 ± 0.0002	1.3 ± 0.2	3.4 ± 0.4
	r	0.9194 ± 0.0007	1.3 ± 0.2	0.8 ± 0.3
		Mg XI		
	f	1.3311 (fixed)	2.3 ± 0.5	$0.08^{+0.11}_{-0.08}$
MEG	i	1.3429 ± 0.0005	2.3 ± 0.5	1.06 ± 0.14
	r	1.3523 (fixed)	2.3 ± 0.5	$0.23^{+0.15}_{-0.10}$

NOTE — Centroid, width, and intensity of the He-like transition lines. The errors associated with each parameter are at 1 σ c. l..

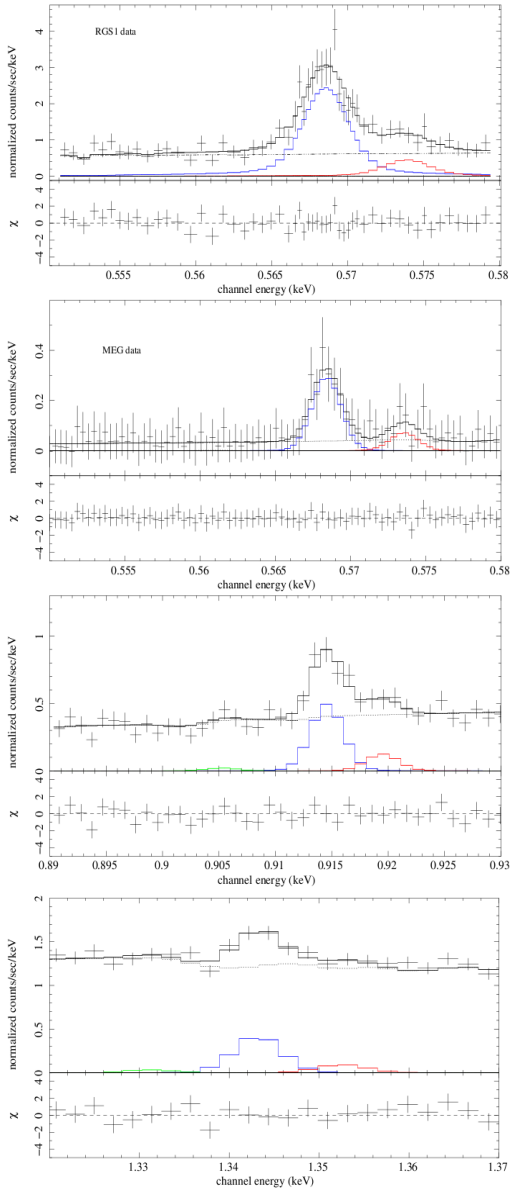

Forbidden (green), intercombination (blue), and resonance (red) lines of the O VII, Ne IX and Mg XI triplets. From the top to the bottom: RGS1 data and residuals of the O VII triplet; first-order MEG data and residuals of the O VII triplet; first-order MEG data and residuals of the Ne IX triplet; first-order MEG data and residuals of the Mg XI triplet.

Plasma diagnostics from He-like triplets

Intercombination lines dominate in triplets over resonant and forbidden lines.

- The R parameter ($= f/i$) is < 0.2 for all the triplets.
- The G parameter ($= (f + i)/r$) is 5^{+13}_{-2}, 5^{+4}_{-2}, and 5^{+6}_{-3} for O VII, Ne IX and Mg XI, respectively.
- Assuming that the lines originate in the same medium we derived:
- **Plasma electron density estimate:** $> \mathbf{10^{14}\ cm^{-3}}$
- **Plasma temperature estimate:** $< \mathbf{5 \times 10^5\ K}$

Emission measures of the photoionised plasma

Ion	α $cm^3\ s^{-1}$	f	$n_e^2 V$ $(10^{56}\ cm^{-3})$
O VII	5.9×10^{-12}	0.84	5 ± 2
O VIII	9.1×10^{-12}	0.16	5 ± 2
Ne IX	1.1×10^{-11}	0.72	3.0 ± 0.7
Ne X	1.5×10^{-11}	0.28	3.0 ± 0.7
Mg XI	1.7×10^{-11}	0.71	2.1 ± 0.5
Mg XII	2.3×10^{-11}	0.29	2.1 ± 0.5
Si XIII	2.5×10^{-11}	0.49	0.8 ± 0.2
Si XIV	3.3×10^{-11}	0.52	0.8 ± 0.2

NOTE — The fractional numbers of ions in the given ionisation state is reported in second column. The emission measure is reported in the third column.

Emission measure

We also estimated the emission measure of different elements using the ratio of He-like/H-line line intensities and cosmic abundances. The emission measure values have all the same order of magnitude of $\sim 10^{56}\ cm^{-3}$.

dsfa

Conclusions

Results

- The most updated ephemeris of X1822-371 ($\dot{P}$ = 1.591(86) $\times$ 10^{-10} s/s).
- A first measure of time lag (optical vs. X-ray) and optical-UV modulation
- Constraints based on a simplified model of density, size and pulsed fraction in the ADC
- Chandra and XMM-Newton spectra are consistently well fitted by an optically thick Comptonized emission, partially (fraction 60%) occulted by a torus-like medium of neutral matter of equivalent hydrogen column of 3.5$\times$ 10^{22} cm^{-2}.
- The spectrum shows several emission lines of highly ionized elements (from He- and H-like elements). We identified the triplet complexes of O VII, Ne IX and Mg XI, from which we derived density and temperature of the plasma emitting lines.
- A two-phase corona is the most realistic scenario to explain the data